Transmission Improvement in Ultralong Dispersion-Managed Soliton WDM Systems by Using Pulses With Different Widths

T. I. Lakoba

***Abstract*—It was shown that one can improve transmission performance in ultra-long-haul wavelength-division-multiplexed (WDM) systems by matching the input pulsewidth to the path-averaged dispersion (PAD) in the line. Wider pulses should be used for higher values of PAD, and vice versa. It was also noted that this pulsewidth selection is only effective in the dispersion-managed soliton (DMS) propagation regime but not in the chirped return-to-zero (CRZ) regime.**

***Index Terms*—Optical fiber communication, optical pulses.**

I. Introduction

In modern long-haul transmission systems, pulses propagate in a dispersion map, where most of the dispersion accumulated over each span of transmission fiber is compensated by a dispersion-compensating module (DCM). The uncompensated part of the accumulated dispersion, averaged over the span length, is referred to as the path-averaged dispersion (PAD). In wavelength-division-multiplexed (WDM) systems that use a single DCM for channels occupying the bandwidth of a few tens of nanometers, the PAD usually varies with wavelength due to a mismatch between dispersion slopes of the transmission and dispersion-compensating fibers. In such a case, two channels located sufficiently far apart within the band may "see" values of PAD that differ by a factor of order 2. One way to make the PAD more uniform among the channels is to subdivide the entire wavelength band into smaller subbands and then use separate DCMs for each subband. However, this approach has the disadvantage of increasing both the cost and the footprint of the transmission system.

The reason one would tend to avoid having uncompensated PAD is that it causes dispersive pulse broadening, accumulation of chirp, and distortions of the pulse shape. Under certain conditions, these effects of PAD can be compensated for by the pulse's self-phase modulation (SPM), which occurs due to the nonlinearity of the fiber refractive index. Whenever such a balance between the PAD and SPM is attained, the pulse parameters, such as temporal and spectral widths, chirp, and peak power (approximately) repeat themselves at every span of the dispersion map. The corresponding pulse is then referred to as a dispersion-managed soliton (DMS). A DMS has a specific value of prechirp (i.e., dispersion precompensation) at the system's input, as well as a certain relation among its power, temporal width, and the PAD (see, e.g., [1] and references therein). However, as noted above, for channels whose wavelengths are sufficiently far apart, the respective values of PAD may differ by a factor of order 2. For a given dispersion map, those values are fixed. Moreover, the power $P_{\rm ch}$ of a channel is set by the requirement to achieve a certain optical signal-to-noise ratio (OSNR) at the receiver, and thus, is also fixed for the given system. It is not always possible or advisable to tailor $P_{\rm ch}$ so that it would follow the profile of the PAD as a function of wavelength; in fact, in most cases, $P_{\rm ch}$ is kept the same for all channels. Thus, with a fixed value for $P_{\rm ch}$, the balance between the PAD and SPM, which is required to support a DMS, can be achieved only if pulses in channels "seeing" different PAD are launched with accordingly different widths. Specifically, pulses propagating at a smaller PAD should have a smaller input width, and vice versa.

In this paper, we present results of numerical simulations that demonstrate that one can indeed improve performance of ultra-long-haul transmission systems by using properly selected pulsewidth for pulses propagating at different values of the PAD. The main reason for this improvement is the (approximate) balance between the dispersive and nonlinear effects that helps maintain a stationarily propagating pulse, as discussed previously. However, there are three aspects in which the results go beyond being just a trivial corollary of the aforementioned condition to have a DMS in the transmission line. First, the latter condition was derived for the infinite propagation distance. To the author's knowledge, distortions of a pulse that does not satisfy the DMS condition and the system impact of such distortions have not previously been systematically and quantitatively assessed. In this paper, such an assessment for a particular transmission system is provided, and it is shown that the benefit of using pulses with properly selected widths becomes compelling for systems that are longer than 3000 km. Second, selecting a pulsewidth so as to attempt to satisfy the DMS condition may lead to the deterioration of the system performance with respect to other factors. Those factors include, e.g., 1) a decreased eye opening due to a lower peak power of wider initial pulses and 2) increased intra- or interchannel pulse interaction, which may lead to timing jitter. It is demonstrated here that, for transmission distances of up to 4000 km, the detrimental effect of those factors is much less important than the positive effect

Manuscript received February 11, 2004; revised January 7, 2005.

The author is with the Department of Mathematics and Statistics, University of Vermont, Burlington, VT 05405 USA.

Digital Object Identifier 10.1109/JLT.2005.851333

of the restored balance between the PAD and SPM, which can be achieved by using wider pulses for higher values of PAD. Finally, it is noted that pulsewidth management can be readily implemented in a commercial transmission system by employing a tunable-pulsewidth transmitter. Specifically, the efficiency of the pulsewidth selection principle proposed in this paper has recently been demonstrated experimentally [2], [3], as discussed in more detail in Section III.

The remainder of this paper is organized as follows. Section II describes the results of the semianalytical variational method and direct numerical simulations for an isolated pulse in a single channel. These results confirm the earlier claim that wider input pulses suffer less distortion when propagating at larger values of the PAD. Section III extends these results to a WDM case and demonstrates that the system performance is improved when the pulsewidth is chosen in accordance with the PAD value. To quantify this improvement, multichannel simulations for a particular ultra-long-haul terrestrial system, which have been described in [2] and [3], are performed. It is shown that, for this and similar systems, the benefit of restoring the balance between the SPM and PAD by using wider pulses for larger values of PAD greatly outweighs all degradations that the wider pulses may suffer compared with the narrower ones. Finally, the author comments on the difference between the DMS and chirped return-to-zero (CRZ) regimes with respect to the pulsewidth selection.

II. Single-Channel Results

In this section, we present results that show two main mechanisms of degradation of a pulse for which the balance between the PAD and SPM does not hold. These mechanisms are 1) the change of the pulse's minimum width and 2) a strong dependence on the PAD of the amount of dispersion postcompensation that is required to obtain a pulse with the maximum peak power at the receiver.

The pulse propagation in the transmission system is modeled by the nonlinear Schrödinger equation (NLS)

$$i\frac{\partial u}{\partial z}+\frac{\lambda^2}{4\pi c}D\frac{\partial^2 u}{\partial t^2}+P_0G(z)u|u|^2=0. \tag{1}$$

Here, z is the propagation distance, λ and c are the carrier wavelength and the light speed in vacuum, respectively, D is the dispersion coefficient that equals D_1 in the transmission fiber ($0\le \mathrm{mod}(z,L_{\mathrm{map}})<L_1$) and equals D_2 in the DCM ($L_1\le \mathrm{mod}(z,L_{\mathrm{map}})<L_{\mathrm{map}}$), $L_{\mathrm{map}}=L_1+L_2$ is the period of the dispersion map, t is the delayed time, P_0 and $P_0|u|^2$ are the peak and instantaneous pulse powers at the input to each span, respectively, and $G(z)=\gamma P_0(z)/P_0$, where $\gamma=\gamma_1$ or $\gamma=\gamma_2$ (with $\gamma_{1,2}$ being the nonlinear coefficients of the transmission fiber and the DCM) and the factor $P_0(z)/P_0$ characterizes the pulse power evolution due to loss and periodic amplification. Note that the pulse peak power P_0 is related to the launched channel power P_{ch} as $P_{\mathrm{ch}}=P_0\int_0^{T_{\mathrm{bit}}}|u(t,z=0)|^2\mathrm{d}t/(2T_{\mathrm{bit}})$, where T_{bit} is the bit duration.

The particular transmission system, which has been described in detail in [3], is considered. It consists of up to 40 100-km spans of TrueWave reduced slope (TWRS) fiber, compensated by DCMs that provide PAD values of approximately 0.14 and 0.36 ps/nm/km for channels propagating at 1550 and 1580 nm, respectively. The dispersion of TWRS equals approximately 4.5 and 6.0 ps/nm/km at those wavelengths. The precompensation is provided by a single DCM for all channels, with the value of the optimal precompensation being discussed below and being taken the same for all channels. The 10-Gb/s channels are located on the 50-GHz grid and have the power of -5 dBm/channel at the beginning of each span. Each span has 23 dB of loss, 20 dB of which is compensated by forward ($\sim$ 3.5 dB) and backward ($\sim$ 16.5 dB) Raman pumping of the transmission fiber. The remaining amplification is provided by the DCM, which is backward Raman pumped. The pulses can have the full-width at half-maximum (FWHM) of either 33 or 50 ps and can have an approximately Gaussian shape (see Section III for details). Here and in what follows, the input pulse width is referred to, unless stated otherwise.

The objective of this section is to determine a range of precompensation values that would optimize the performance of a single channel for both values of PAD simultaneously. Therefore, the quantities computed in this section will be presented as a function of the precompensation. We begin with estimating the width and chirp of an isolated pulse at the optical output (i.e., after the fortieth span but before the receiver) of the above transmission system. To that end, we employ the variational method with the pulse shape being modeled by a Gaussian

$$u=\frac{\sqrt{P_0}}{\sqrt{1+\frac{i\Delta}{\tau_0^2}}}\exp\left[-\frac{t^2\left(1-\frac{i\Delta}{\tau_0^2}\right)}{2\tau_0^2T_{\mathrm{DM}}^2\left(1+\frac{\Delta^2}{\tau_0^4}\right)}\right] \tag{2}$$

where [1] τ_0 is the nondimensional minimum width, which is related to the FWHM as: $\mathrm{FWHM}=2\sqrt{\ln 2}\tau_0T_{\mathrm{DM}}$, where $T_{\mathrm{DM}}=[\lambda^2/(2\pi c)|D_1-D_2|L_1L_2/L_{\mathrm{map}}]^{1/2}$ is the time normalization parameter. Furthermore, the chirp parameter $\Delta(z)=\Delta_0+(1/L_{\mathrm{map}})\int_0^z \mathrm{d}(z')\mathrm{d}z'$, where

$$\mathrm{d}(z)=\begin{cases}\mathrm{sgn}(D_1)\frac{L_{\mathrm{map}}}{L_1}, & 0\le z<L_1\\ -\mathrm{sgn}(D_1)\frac{L_{\mathrm{map}}}{L_2}, & L_1\le z<L_{\mathrm{map}}\end{cases}$$

is the nondimensional dispersion coefficient with zero average ($\int_0^{L_{\mathrm{map}}}\mathrm{d}(z')\mathrm{d}z'=0$). Note that the nondimensional parameter Δ_0 is related to the dimensional precompensation value $\delta_{\mathrm{precomp}}$ as follows: $\delta_{\mathrm{precomp}}=\Delta_0T_{\mathrm{DM}}^2(2\pi c/\lambda^2)$.

The parameters of an isolated pulse (2) undergo the following slow evolution caused by the PAD and SPM (see, e.g., [4])

$$\frac{\mathrm{d}\tau_0}{\mathrm{d}z}=\frac{2P_{\mathrm{ch}}G(z)\Delta(z)}{\sqrt{2\pi}\left(\frac{T_{\mathrm{DM}}}{T_{\mathrm{bit}}}\right)\tau_0^2\sqrt{1+\frac{\Delta^2}{\tau_0^4}}^3} \tag{3a}$$

$$\frac{\mathrm{d}\Delta_0}{\mathrm{d}z}=\frac{\lambda^2}{2\pi c}\frac{D_{\mathrm{av}}}{T_{\mathrm{DM}}^2}-\frac{2P_{\mathrm{ch}}G(z)\tau_0\left(1-\frac{\Delta^2}{\tau_0^4}\right)}{\sqrt{2\pi}\left(\frac{T_{\mathrm{DM}}}{T_{\mathrm{bit}}}\right)\sqrt{1+\frac{\Delta^2}{\tau_0^4}}^3} \tag{3b}$$

where $D_{\mathrm{av}}=(D_1L_1+D_2L_2)/L_{\mathrm{map}}$ is the PAD. The coupled equations (3a) and (3b) are solved numerically over 4000 km of the transmission fiber. The output pulse minimum width

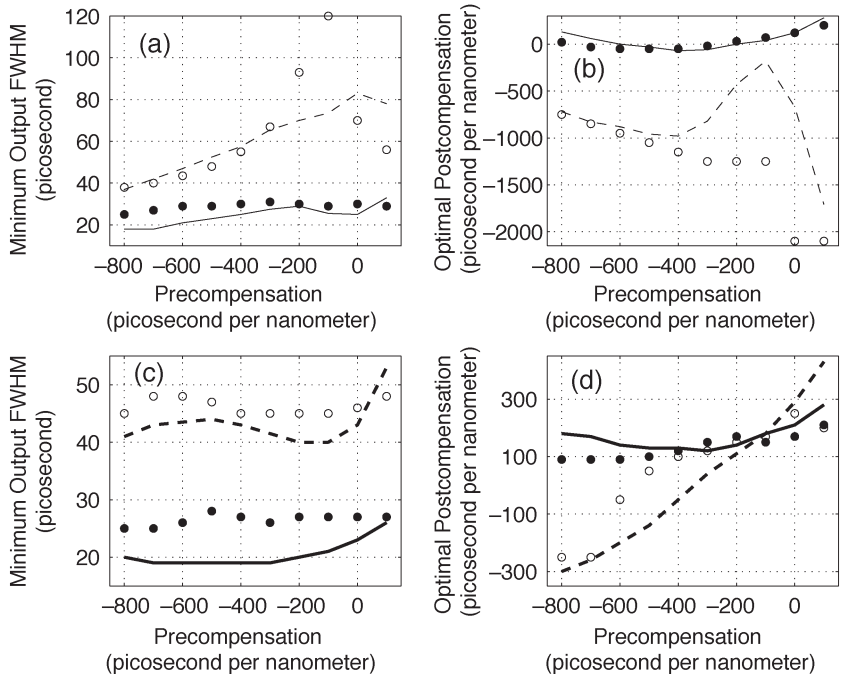

Fig. 1. (a, c) Minimum width of the output pulse and (b, d) the optimal postcompensation for which the pulse with the minimum width is obtained, after 4000 km. In (a, b), thin solid and dashed lines show the variational results for the 33-ps pulses propagated at 1550 nm (low PAD) and 1580 nm (high PAD), respectively. In (c, d), thick solid and dashed lines show the variational results for the 50-ps pulses propagated at 1550 nm (low PAD) and 1580 nm (high PAD), respectively. In all plots, filled and empty circles show the results of direct numerical simulations for a single pulse at 1550 and 1580 nm, respectively.

and the postcompensation required to obtain a chirp-free pulse, as functions of dispersion precompensation at the input to the system, are plotted in Fig. 1. We emphasize that the changes of the minimum width from the system's input to the output, shown in Fig. 1(a) and (c), occur due to an interplay between the PAD and SPM along the fiber. Thus, this is an essentially nonlinear effect and should not be confused with a purely linear dispersive pulse broadening.

An interpretation of the variational results shown in Fig. 1 is given as follows: For a 33-ps pulse near 1550 nm, a PAD of 0.14 ps/nm/km is somewhat smaller than that required to support a DMS. Hence, the slight narrowing, observed in Fig. 1(a), of the pulse is caused by the part of the SPM that is not compensated by the PAD (see, e.g., [5]). Similarly, the variational method predicts that the output FWHM of an initially 33-ps pulse launched at 1580 nm, where the PAD ($= 0.36$ ps/nm/km) is too high for a DMS, increases by more than a factor of 2. As already noted, this pulse broadening is a nonlinear effect and cannot be undone by any linear dispersion postcompensation at the receiver. Thus, the corresponding eye opening irreversibly decreases compared to that at the system's input. Moreover, the difference between the optimal values of postcompensation for channels transmitted at 1550 and 1580 nm exceeds 500 ps/nm for all values of precompensation except those in a narrow region between -200 and 0 ps/nm; see Fig. 1(b). No single fiber-based DCM is capable of providing postcompensation that would differ by that amount for the aforementioned channels, and any attempt to use a compromise value of postcompensation would lead to suboptimal pulse width, and thus, further degrade the eye opening.

The situation is dramatically improved if instead of 33-ps pulses, one launches 50-ps pulses in channels seeing a PAD of 0.36 ps/nm/km. According to the variational method, the output pulses then have the minimum width between 40 and 50 ps for precompensation values considered. Moreover, for the precompensation above -600 ps/nm, the postcompensation required to obtain bandwidth-limited pulses in this case differs by less than 200 ps/nm from the postcompensation required for the 33-ps pulses launched at a PAD of 0.14 ps/nm/km [compare the thick dashed line in Fig. 1(d) and the thin solid line in Fig. 1(b)].

To verify the results of the variational method, the propagation of an isolated pulse in (1) was numerically simulated. The optimal postcompensation values, for which the output peak power of the pulse is the maximum, are presented in Fig. 1(b) and (d). At those values of postcompensation, the FWHM of the output pulse is measured and plotted in Fig. 1(a) and (c). We note that the necessary condition for the numerical and variational results to agree is the output pulse width being close to the input pulse, as confirmed in Fig. 1. The reason behind this is the following: An actual pulse anywhere inside the fiber can be represented as a superposition of Hermite–Gaussian harmonics [6], of which the variational method captures only the zeroth- and second-order ones, corresponding to the changes of the pulsewidth and chirp (a change of the peak power is related to the change of the width via the energy conservation: $P_0\tau_0 = \text{const}$). Whenever there is a balance between the SPM and PAD, the second- and higher order Hermite–Gaussian harmonics can be shown [7], [8] to remain small. On the other hand, when either of the SPM and PAD dominates over the other, the zeroth-order harmonic causes the second- and higher order ones to grow. This leads to a significant change of the pulsewidth and to the output pulse shape becoming non-Gaussian. These effects, for the 33-ps

pulses launched at $D_{\rm av} = 0.36$ ps/nm/km with precompensation values of -400 ps/nm/km and above, are observed in Fig. 1(a) and (b)—for the output pulsewidth and chirp—and in Fig. 3(e)—for the non-Gaussian shape of an isolated output pulse. On the contrary, 50-ps pulses launched at this PAD exhibit much less change in their output width and shape, and hence, the variational and numerical results for those pulses agree reasonably well with each other. We also conclude from Fig. 1(a) and (b) that for $D_{\rm av} = 0.14$ ps/nm/km, 33-ps pulses launched with precompensation values between -500 and 0 ps/nm exhibit only small changes to their output width and shape.

The above considerations can be summarized as follows: For precompensation above -500 ps/nm, the use of 33-ps pulses in the channels propagating at 1580 nm and the higher PAD is precluded by the substantial amount of distortion suffered by these pulses. For precompensation values below -500 ps/nm, the output pulses are fairly undistorted, but their optimal postcompensation differs by about 800 ps/nm from that required for similar pulses propagated at 1550 nm and the lower PAD [see Fig. 1(b)]. That would necessitate having to use separate DCMs for the 1550- and 1580-nm channels if both of the channels were to employ 33-ps pulses. However, if one uses 33-ps pulses in the channels "seeing" the lower PAD and 50-ps pulses in the channels "seeing" the higher PAD, then for the precompensation values between -500 and -200 ps/nm/km (according to the numerical results shown in Fig. 1), the pulses in both groups of channels appear to suffer little distortion and require similar amounts of postcompensation for optimal performance.

The specific value of optimal precompensation has to be obtained from direct multichannel simulations of the NLS (1). In addition to the considerations presented above, the optimal precompensation is also determined by the requirements that the timing jitter resulting from interchannel cross-phase modulation (XPM), which is the main impairment for DMS-based systems [9], be minimized simultaneously for all channels. For the transmission system described above, such a precompensation turns out to be near -300 ps/nm. This is the value used in Section III.

III. Multichannel Results

Transmission of two groups of five 10-Gb/s 50-GHz-spaced channels at 1550 and 1580 nm was simulated. Each channel contains the same $(2^7 - 1)$-bit-long pseudorandom bit sequence (PRBS), with the PRBSs in consecutive channels being time shifted relative to one another by 23.7, 23.9, 24.1, and 24.3 bits. Among several time-shifting sequences that we used, the above one led to the maximum worst case timing jitter induced by the interchannel XPM. All channels have the same time-averaged power of -5 dBm, as in Section II. At the receiver, the pulses are demultiplexed by a filter with a 32-GHz optical bandwidth and then detected by a receiver with a fourth-order Bessel characteristic and an electrical bandwidth of 7.5 GHz. Other parameters of the simulations are the same as in Section II.

The amplified spontaneous emission (ASE) is not included in the transmission simulations and is added, instead, at the receiver, as explained later. The primary effect of adding the ASE inline would have been the Gordon–Haus (GH) timing jitter [10]. However, in 10-Gb/s dispersion-managed systems for terrestrial applications, this effect is quite small due to a relatively short distance and small PAD. To estimate it, we used the result of [11], where the GH jitter in a system similar to the one considered here was calculated. Rescaling that result by using the well-known dependence of the GH jitter on the pulsewidth and energy and on the system amplifier gain and PAD (see, e.g., [12]), we find the root-mean-square GH jitter at the receiver for the 33-ps pulses and a PAD of 0.36 ps/nm/km to be about 2 ps (i.e., 4 ps peak to peak). For the 50-ps pulses, it is smaller by a factor of (50/33) ≈ 1.6. In both cases, the GH jitter at the receiver can be reduced by using slightly more negative postcompensation than that provided by the inline DCM. Thus, the magnitude of the GH jitter in this case is substantially smaller than that of the XPM-induced timing jitter (see later discussion) and does not alter the conclusions of this study.

We now briefly describe how input pulses of different widths are generated in the simulations.[1] The transmitter is modeled as a dual-stage Mach–Zehnder interferometer (MZI). Its first stage, the pulse carver, produces a stream of return-to-zero pulses separated by the bit period, while the second stage imposes pseudorandom data onto that stream. The pulsewidth is set by the first stage; namely, its output power $P(t)$ is

$$P(t) = P_0 \cos^2\left(\arccos\left(\frac{1}{\sqrt{C}}\right)\sin\left(\frac{\pi t}{T_{\rm bit}}\right)\right). \qquad (4)$$

The parameter C is the contrast ratio (i.e., the ratio between the maximum and minimum powers) of the MZI output. It also controls the pulsewidth: e.g., $C = \infty$ (infinite contrast ratio) corresponds to nearly Gaussian pulses with FWHM of $0.33T_{\rm bit}$, while $C = 0.2$ yields $0.5T_{\rm bit}$-wide pulses with 7 dB of contrast ratio. As realistic values for the data modulator (i.e., the second stage of the MZI), an extinction ratio between ONEs and ZEROs was chosen to be 13 dB and the modulator's RF driver was chosen to have a bandwidth of 12 GHz.

As a performance metric, we choose the OSNR (in 0.1 nm) required to achieve a given target bit error rate (BER). This metric can be used to calculate both the OSNR margin as

$$\text{OSNR Margin} = \text{Received OSNR} - \text{Required OSNR After Transmission}$$

and the transmission penalty as

$$\text{Transmission Penalty} = \text{Required OSNR After Transmission} - \text{Required OSNR Back to Back.}$$

The concept of transmission penalty can be viewed as an extension of the power penalty concept in linear systems [5]

[1] Although the experiments reported in [2] and [3] used a different transmitter than the one described below, the primary difference between these two transmitters is not in performance but in the economics of the device.

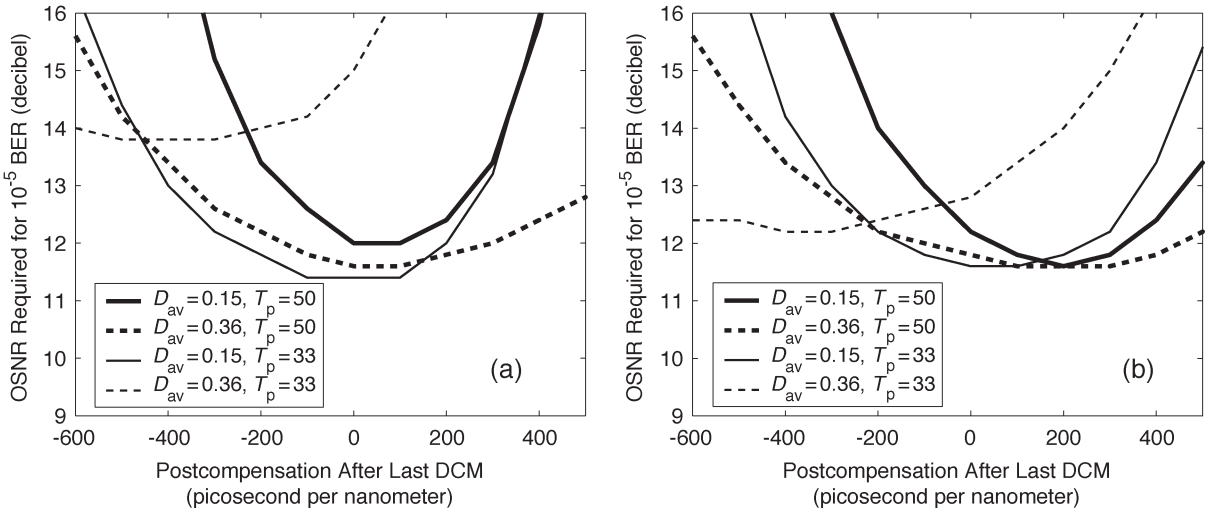

Fig. 2. OSNR required to achieve $\mathrm{BER} = 10^{-5}$ after transmission over (a) 4000 km and (b) 3000 km. Notations are the same as in Fig. 1. Precompensation is -300 ps/nm, and the results for the worst of the five channels are shown. For reference, OSNRs required for the 10^{-5} BER before transmission are 11.4 and 12.4 dB for the 33- and 50-ps pulses, respectively.

to systems impaired by nonlinearity. For a given OSNR value, the BER is estimated by adding the ASE to the signal at the receiver, as in, e.g., [13]; 10^{-5} is chosen as the target BER value. This is relevant to real systems that use forward-error correction to bring that high BER down to around 10^{-16}.

Fig. 2 shows the OSNR required to achieve the BER of 10^{-5} after transmission over 4000 and 3000 km for each of the simulated cases as a function of postcompensation added after the last inline DCM. (For reference, the OSNRs required for the 10^{-5} BER before transmission are about 11.4 and 12.4 dB for the 33- and 50-ps pulses, respectively.) Two conclusions can be drawn from Fig. 2(a) (4000 km). First, for the higher value of PAD, the minimum achievable penalty is ~ -0.8 dB for the 50-ps pulses and $\sim$ 2.4 dB for the 33-ps ones. The corresponding electrical eye diagrams are shown in Fig. 3(b) and (d). Fig. 3(e) shows that at the optimal postcompensation for the entire channel, the isolated pulses broaden the most while pulses coming in groups broaden much less. In Fig. 3(b), the isolated pulses form the lower trace of the eye diagram. Thus, the principal source of transmission penalty for the 33-ps pulses at high PAD is the broadening of isolated pulses, as discussed in Section II.

The second conclusion that follows from Fig. 2(a) concerns the range of postcompensation values that are optimal for channels at 1550 and 1580 nm simultaneously. Namely, when 33-ps pulses are used for both lower and higher values of PAD, the optimal postcompensation range is a very narrow vicinity around -450 ps/nm (where the solid and dashed thin lines intersect), and at that optimal postcompensation, the transmission penalty is 2.4 dB. This is to be compared with the case where 33-ps and 50-ps pulses are launched at $D_{\mathrm{av}} = 0.14$ and 0.36 ps/nm/km, respectively. Then, the range of simultaneously optimal postcompensation values is between about -50 and $+150$ ps/nm, which is rather wide. Moreover, in that range, the transmission penalties are about 0 and -0.8 dB for the narrower and wider input pulses, respectively. Thus, Fig. 2(a) confirms the conclusion in Section II that a single postcompensating DCM can easily provide good performance for all channels between 1550 and 1580 nm if the pulsewidth is chosen in accordance with the PAD rather than uniformly for all channels.

We note that the benefit of using wider input pulses at higher values of PAD greatly overweighs the disadvantages of such an approach. Specifically, Fig. 3(d) shows that the main such disadvantage is the increased XPM-induced timing jitter of the wider input pulses. It is estimated in Fig. 3(b) and (d) that this jitter is about 12 and 25 ps peak to peak for the 33- and 50-ps pulses, respectively. Nevertheless, the electrical eye for the wider input pulses still has both: 1) a higher value at the ONE level and 2) a lower value at the ZERO level, and hence, it is more open than the eye for the 33-ps pulses. The former improvement, the higher value at the ONE level, has already been related to the results in Section II. The latter improvement, i.e., the "cleaner" ZERO level in Fig. 3(d) compared with that in Fig. 3(b), can also be explained along similar lines. Namely, significantly broadened pulses in Fig. 3(b) extend their "tails" into the adjacent bit slots, thereby causing intersymbol interference.

To conclude the discussion on the 4000-km results, we verified that for the BER of 10^{-9}, which is usually targeted in test-bed transmission experiments, the gain in required OSNR, achieved by using wider pulses at $D_{\mathrm{av}} = 0.36$ ps/nm/km, increases from 2.4 to about 3.6 dB. We also note that an experimental confirmation of the transmission improvement by using wider pulses at higher values of PAD is presented in [2] and [3]. In particular, [3, Fig. 3] shows that the transmission penalty experienced by the 33-ps input pulses at 1580 nm is about 2 dB higher than that experienced by the 50-ps ones. Similarly, [2, Fig. 4] shows that the BER at this wavelength is two orders of magnitude higher for the 36-ps input pulses than for the 48-ps pulses.

The results for the 3000-km propagation, shown in Fig. 2(b), exhibit a much weaker dependence of the transmission penalty on the pulsewidth. In this case, 33-ps pulses suffer only about 1 dB of penalty at the value of postcompensation that is

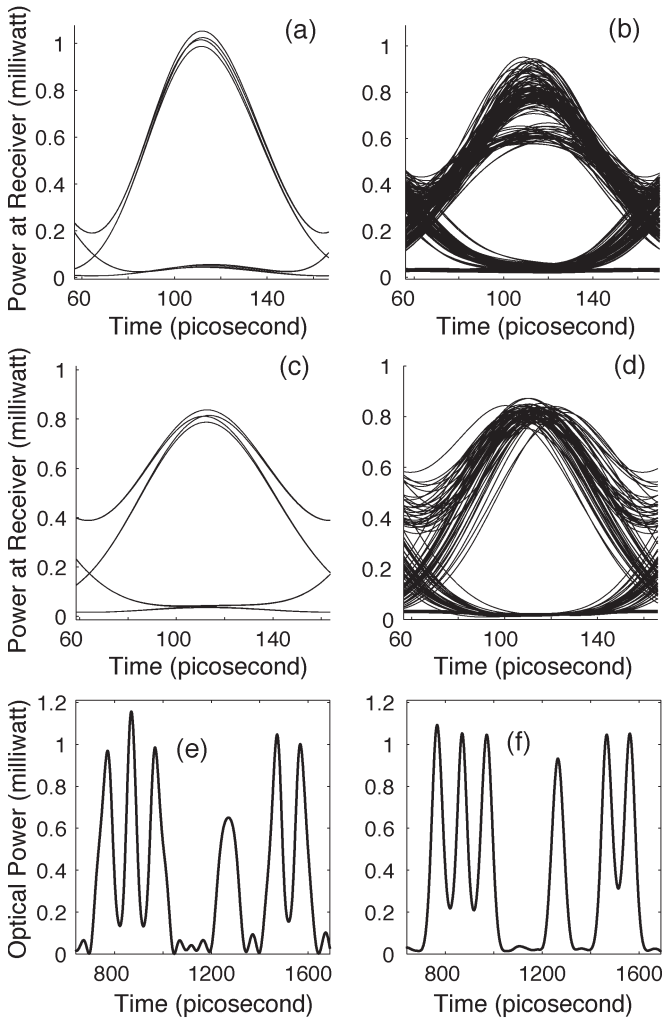

Fig. 3. Electrical eye diagrams for the 33-ps pulses (a) at the input and (b) after transmission over 4000 km at $D_{\rm av} = 0.36$ ps/nm/km and optimal postcompensation. Precompensation is -300 ps/nm/km, and the diagram for the worst of the five channels is shown. Plots (c) and (d) show the corresponding input and output eye diagrams for the 50-ps pulses. Plots (e) and (f) show segments of the optical waveform from which the electrical eye diagrams in, respectively, (b) and (d) were obtained.

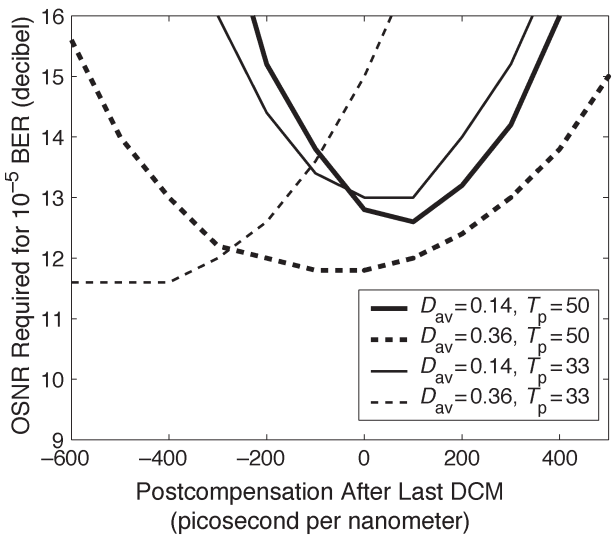

Fig. 4. Same as Fig. 2(a), but precompensation is -900 ps/nm.

simultaneously optimized for both the lower and higher PAD "seeing" channels. Note, however, that the corresponding range of postcompensation values is quite narrow: Deviating from it by 100 ps/nm would increase the penalty of the worst channel by another ~ 0.5 dB. If, on the other hand, one uses 50-ps pulses in the channel transmitted at $D_{\rm av} = 0.36$ ps/nm/km, the corresponding postcompensation range is at least twice as wide. Therefore, the benefit of choosing the pulsewidth in accordance with the PAD may become nonnegligible even for a 3000-km-long system. Furthermore, we verified that at 2000 km, the 33- and 50-ps pulses propagating at $D_{\rm av} = 0.36$ ps/nm/km exhibit nearly equal required OSNR. In this case, a higher transmission penalty suffered by the 33-ps pulses is compensated by their lower required OSNR at the input, the latter being the consequence of the narrower pulses having a higher power at the detection point [see Fig. 3(a) and (c)]. Thus, for a 2000-km-long system, there appear to be no benefits of using pulses with different widths, at least for the range of PAD values considered here.

Now we will clarify a possibly counterintuitive observation, made from Fig. 2, that 50-ps pulses suffer practically no or even negative transmission penalty after 4000 km of propagation in a nonlinear fiber. A similar observation also holds for the 33-ps pulses transmitted at $D_{\rm av} = 0.14$ ps/nm/km, which exhibit no penalty at the optimal postcompensation. We analyzed the eye diagrams corresponding to the aforementioned cases and concluded that the main reason for this effect is that the extinction ratio of the output pulses is higher than that of the input ones. Specifically, after 4000 km, it increases by almost 2 dB for the 50-ps pulses transmitted at $D_{\rm av} = 0.36$ ps/nm/km and by roughly 0.5–1 dB for the 50- and 33-ps pulses transmitted at the lower value of PAD. This is to be expected, as the small pulses located at ZERO bits are practically linear, and thus, get broadened by the accumulated PAD. (The increase in the extinction ratio may also be attributed in part to intersymbol interference, but the latter effect is much less amenable to quantitative estimation.) We performed additional simulations, where we varied the extinction ratio of the optical input from 16 to 12 dB, and observed similar results. Another, but probably less important, reason for the penalty decrease is that (most of) the output pulses are narrower, and hence, taller, than the input ones, which is consistent with the results shown by the solid lines in Fig. 1(a) and (c).

Finally, we emphasize that the improvement of transmission by selecting the pulsewidth according to the PAD "seen" by pulses is efficient only in the DMS regime. In another widely used transmission regime, the chirped return-to-zero (CRZ) pulses are initially strongly prechirped by either a phase modulator or a highly dispersive fiber. This strong prechirp leads to large linear broadening of the pulse at the beginning of the transmission link, and thus, considerably reduces the pulse's SPM [see (3)]. For example, precompensation of -900 ps/nm spreads a 33-ps pulse by a factor of 3 [5]. The reduction in SPM in this case is quite significant, so that the 33-ps input pulses, propagating at 0.36 ps/nm/km, emerge at the output with almost unchanged minimum width [Fig. 1(a)], and their chirp is almost the same as the one that would occur in the linear transmission. Therefore, there is no reason to expect that

the CRZ transmission for the system considered here would be improved for a PAD of 0.36 ps/nm/km by using wider input pulses. This is confirmed in Fig. 4 (compare the thin and thick dashed curves), which shows the OSNR required for BER of 10^{-5} for exactly the same conditions as in Fig. 2(a), except that the precompensation is -900 ps/nm. We note in passing that the transmission at the lower value of PAD (the solid curves in Fig. 4) is degraded mainly due to the intrachannel XPM-induced timing jitter for the pulses (see, e.g., [14]). To summarize the main idea of this paragraph, it is clear from Fig. 4 that selection of the pulsewidth according to the PAD is, in general, not efficient in the CRZ regime.

IV. Conclusion

In conclusion, it was shown that transmission performance in the DMS regime is improved if pulses propagating at different values of PAD are launched with different temporal widths. Wider pulses should be launched at wavelengths corresponding to higher PAD, and vice versa. The improvement is due to a restored balance between the PAD and SPM of a single pulse, and it is believed to be significant for transmission distances beyond 3000 km.

Acknowledgment

The main part of this paper was completed when the author was with Lucent Technologies, Holmdel, NJ. The author would like to thank D. A. Fishman, Y. H. Kao, and L. Altman for useful discussions and support and T. Lubbe and S. Taeger for their critical reading of the original version of the manuscript. The author would also like to thank two anonymous referees for their constructive criticism.

References

[1] T. I. Lakoba and G. P. Agrawal, "Optimization of the average-dispersion range for long-haul dispersion-managed soliton systems," *J. Lightw. Technol.*, vol. 18, no. 11, pp. 1504–1512, Nov. 2000.

[2] Y. Kao, A. Leven, Y. Baeyens, Y. Chen, D. Grosz, F. Bannon, W. Fang, A. Küng, D. Maywar, T. Lakoba, A. Agarwal, S. Banerjee, and T. Wood, "10 Gb/s soliton generation for ULH transmission using a wideband GaAs pHemt amplifier," in *Proc. Optical Fiber Communication (OFC)*, Atlanta, GA, 2003, pp. 674–675, Paper FF6.

[3] D. F. Grosz, A. Agarwal, S. Banerjee, D. N. Maywar, and A. P. Küng, "All-Raman ultra-long-haul single wideband DWDM transmission systems with OADM capability," *J. Lightw. Technol.*, vol. 22, no. 2, pp. 423–432, Feb. 2004.

[4] T. I. Lakoba, J. Yang, D. J. Kaup, and B. A. Malomed, "Conditions for stationary pulse propagation in strong dispersion-management regime," *Opt. Commun.*, vol. 149, no. 4–6, pp. 366–375, Feb. 1998.

[5] G. P. Agrawal, *Nonlinear Fiber Optics*. San Diego, CA: Academic, 1995, ch. 3 and 4.

[6] P. Lazaridis, G. Debarge, and P. Gallion, "Exact solutions for linear propagation of chirped pulses using a chirped Gauss-Hermite orthogonal basis," *Opt. Lett.*, vol. 22, no. 10, pp. 685–687, May 1997.

[7] S. K. Turitsyn, "Breathing self-similar dynamics and oscillatory tails of the chirped dispersion-managed soliton," *Phys. Rev. E*, vol. 58, no. 2, pp. R1256–R1259, Aug. 1998.

[8] T. I. Lakoba and D. J. Kaup, "Hermite-Gaussian expansion for pulse propagation in strongly dispersion managed fibers," *Phys. Rev. E,* vol. 58, no. 5, pp. 6728–6741, Nov. 1998.

[9] P. V. Mamyshev and L. F. Mollenauer, "Soliton collisions in wavelength-division-multiplexed dispersion-managed systems," *Opt. Lett.*, vol. 24, no. 7, pp. 448–450, Apr. 1999.

[10] J. P. Gordon and H. A. Haus, "Random walk of coherently amplified solitons in optical fiber transmission," *Opt. Lett.*, vol. 11, no. 10, pp. 665–667, Oct. 1986.

[11] C. J. McKinstrie, "Gordon-Haus timing jitter in dispersion-managed systems with distributed amplification," *Opt. Commun.*, vol. 200, no. 1–6, pp. 165–177, Dec. 2001.

[12] N. J. Smith, W. Forysiak, and N. J. Doran, "Reduced Gordon-Haus jitter due to enhanced power solitons in strongly dispersion managed systems," *Electron. Lett.*, vol. 32, no. 22, pp. 2085–2086, Oct. 1996.

[13] P. J. Winzer, M. Pfennigbauer, M. M. Strasser, and W. R. Leeb, "Optimum filter bandwidth for optically preamplified RZ and NRZ receivers," *J. Lightw. Technol.*, vol. 19, no. 9, pp. 1263–1273, Sep. 2001.

[14] R. I. Killey, H. J. Thiele, V. Mikhailov, and P. Bayvel, "Reduction of intrachannel nonlinear distortion in 40-Gb/s-based WDM transmission over standard fiber," *IEEE Photon. Technol. Lett.*, vol. 12, no. 12, pp. 1624–1626, Dec. 2000.

T. I. Lakoba, photograph and biography not available at the time of publication.